Suppression of crystallization in saline drop evaporation on pinning-free surfaces

The Journal of Chemical Physics ARTICLE scitation.org/journal/jcp

Suppression of crystallization in saline drop evaporation on pinning-free surfaces

Cite as: J. Chem. Phys. 158, 124708 (2023); doi: 10.1063/5.0139448
Submitted: 20 December 2022 • Accepted: 6 March 2023 •
Published Online: 23 March 2023

Alex Jenkins, Gary G. Wells,[a] Rodrigo Ledesma-Aguilar, Daniel Orejon, Steven Armstrong, and Glen McHale

AFFILIATIONS

Institute for Multiscale Thermofluids, School of Engineering, The University of Edinburgh, Edinburgh EH9 3FB, United Kingdom

Note: This paper is part of the JCP Special Topic on Chemical Physics of Controlled Wettability and Super Surfaces.
[a]**Author to whom correspondence should be addressed:** gary.wells@ed.ac.uk

ABSTRACT

For sessile droplets of pure liquid on a surface, evaporation depends on surface wettability, the surrounding environment, contact angle hysteresis, and surface roughness. For non-pure liquids, the evaporation characteristics are further complicated by the constituents and impurities within the droplet. For saline solutions, this complication takes the form of a modified partial vapor pressure/water activity caused by the increasing salt concentration as the aqueous solvent evaporates. It is generally thought that droplets on surfaces will crystallize when the saturation concentration is reached, i.e., 26.3% for NaCl in water. This crystallization is initiated by contact with the surface and is thus due to surface roughness and heterogeneities. Recently, smooth, low contact angle hysteresis surfaces have been created by molecular grafting of polymer chains. In this work, we hypothesize that by using these very smooth surfaces to evaporate saline droplets, we can suppress the crystallization caused by the surface interactions and thus achieve constant volume droplets above the saturation concentration. In our experiments, we used several different surfaces to examine the possibility of crystallization suppression. We show that on polymer grafted surfaces, i.e., Slippery Omniphobic Covalently Attached Liquid-like (SOCAL) and polyethyleneglycol (PEGylated) surfaces, we can achieve stable droplets as low as 55% relative humidity at 25 °C with high reproducibility using NaCl in water solutions. We also show that it is possible to achieve stable droplets above the saturation concentration on other surfaces, including superhydrophobic surfaces. We present an analytical model, based on water activity, which accurately describes the final stable volume as a function of the initial salt concentration. These findings are important for heat and mass transfer in relatively low humidity environments.

I. INTRODUCTION

The evaporation of sessile droplets of non-pure liquids is the subject of intense study due to its wide applications in printing,[1] virology,[2] microfluidics,[3] and heat exchangers.[4] Despite this interest, many of the models currently used do not comprehensively cover the evaporation dynamics and predict their behavior given substrate surface properties, fluid composition, and surrounding environment.[5] For all liquids on a surface, the surrounding atmosphere plays a key role in dictating the rate of phase change from liquid to gas. For pure liquids, such as water, this evaporation rate is often limited by the diffusion of the water vapor through the surrounding gas phase.

In non-pure liquids, such as saline solutions, the mechanisms dictating the evaporation rate are more complicated. Since the diffusion-limited evaporation is governed by the relationship between the vapor pressure at the interface and that far away from the droplet, for non-pure liquids, the vapor pressure at the droplet interface must be adapted to capture the effect of the solute. In the work by Soulie *et al.*,[6] a spatiotemporal relationship, $g(c)$ based on the different vapor pressures of the saline solution and that of the pure fluid as well as the ambient relative humidity has been proposed. This relationship can be used to determine a water activity that accurately describes the change in the liquid vapor pressure, which, in turn, dictates the evaporation rate. For example, the addition of salt (and, e.g., solutions of glycerol or sulfuric acid) is used by the food industry to control the water content when drying or packaging food. Saturated salt solutions maintain a constant humidity as long as the amount of salt present is above the saturation level. There is also a critical water activity below which no micro-organisms can grow. For most foods, this is in the 0.6–0.7 water activity range.

Pathogenic bacteria cannot grow below a water activity of 0.85–0.86, whereas yeast and molds are more tolerant to a reduced water activity of 0.80, but usually, no growth occurs below a water activity of about 0.62 (see, e.g., the work of Rahman & Labuza[7]).

In a non-pure liquid, evaporation also changes the balance of the liquid composition so, for example, in a saline drop, salt concentration increases and crystallization may occur under suitable conditions. There are two possible regimes for crystal nucleation: homogeneous and heterogeneous nucleation.[8] Homogeneous crystal nucleation is a random process in which precipitates form a perfect lattice; this is rare and only occurs when the strain and surface energy creating the ionic interactions are small.[9] For sessile droplets, the mechanism for crystallization has been attributed to heterogeneous surface nucleation.[10] Such nucleation involves processes occurring at the solid surface due to surface heterogeneity can be caused by roughness and variations in surface wetting, which can be characterized by contact angle hysteresis.

Recently, smooth surfaces with extremely low contact angle hysteresis (CAH)[11] below 2° have been shown to have such little contact line pinning of droplets of water that the ideal constant contact angle (CCA) mode of evaporation[12] identified by Picknett and Bexon[13] can be observed. The smoothness, attributed to chemical homogeneity, of polymer brush surfaces has previously been seen to have a significant effect in scaling experiments.[17,18] In these studies, the nucleation rate is reported as being proportional to the available number of nucleation sites; therefore, we believe that the surface hysteresis can be used to represent the suppression of salt crystallization. It has also previously been shown that polymer brush surfaces outperform fluorinated coatings for anti-scaling experiments and therefore provide the ideal study for salt crystallization.[19] However, the implication of this for evaporation-induced crystallization with sessile saline drops has not been considered.

In this work, we aim to reduce the heterogeneity of the surface that allows for crystals to form during the evaporation of sessile saline droplets by evaporating in the CCA mode. By suppressing these mechanisms, we show that a sessile saline droplet's evaporation behavior is eventually dominated by the effect of the solute on the water activity at the liquid–vapor interface. In this regime, stable droplets that stop evaporating under controlled environmental conditions without crystallization are created. This phenomenon has previously been seen in levitating droplets[14,15] but with the crucial difference of a lack of contact with a solid surface. The surfaces shown in the work of Armstrong *et al.*[12] show no contact line pinning and a contact angle (CA) of ~105°. Here, we use the same surface properties to attain behavior similar to evaporating levitating saline droplets but for sessile saline droplets on a surface. We also use other surfaces and see similar behavior, specifically for other low CAH surfaces such as PEGylated surfaces but for sessile saline droplets on a solid surface.[16]

II. THEORETICAL DEVELOPMENT

A. Picknett and Bexon model for sessile droplets of water

When the size of a droplet is much less than the capillary length of the evaporating liquid, $\kappa^{-1} = (\gamma_{LV}/\rho g)^{1/2}$, where γ_{LV} is the surface tension, ρ is the density of the liquid, and g is the acceleration due to gravity, the droplet adopts a spherical cap shape. For a given volume of liquid, V, there are then well-defined geometric parameters, the spherical radius R, contact radius r, and contact angle, θ, which can be measured from side profile images. Geometrically, these parameters are related by

$$r = R \sin\theta \tag{1}$$

and

$$V = \frac{\pi\beta(\theta)R^3}{3}, \tag{2}$$

where

$$\beta(\theta) = 2 - 3\cos\theta + \cos^3\theta = (1-\cos\theta)^2(2+\cos\theta). \tag{3}$$

In general, the rate for diffusion-limited loss of a liquid mass by evaporation through a liquid–vapor interface is

$$\frac{dm}{dt} = -D\int \underline{\nabla} C \cdot \underline{dS}, \tag{4}$$

where D is the diffusion coefficient of the vapor and C is the concentration of the vapor. Combining the geometrical assumptions with Eq. (4) and a concentration gradient model allows data on the evaporation of sessile droplets to be analyzed.

Picknett and Bexon[13] provided an exact solution for Eq. (4) for sessile droplets assuming constant temperature (isothermal model) in the form of an infinite series and provided interpolation formulas using a power series in the contact angle, one for $0^\circ \le \theta < 10^\circ$ and a second for $10^\circ \le \theta \le 180^\circ$, to provide simple evaluation. Subsequently, Stauber *et al.*[20] provided an alternative solution using an integral formulation. Erbil *et al.*[21] considered the Picknett and Bexon solution and introduced a function $f(\theta)$ to take account in a common notational format of the dependence of the concentration gradient of the vapor, between the surface of the droplet and its surroundings, on the contact angle arising from different models,

$$\begin{aligned}\frac{dm}{dt} &= -4\pi D c_s(1-H_r)Rf(\theta)\\ &= -4\pi D c_s(1-H_r)\left(\frac{3V}{\pi\beta(\theta)}\right)^{1/3} f(\theta),\end{aligned} \tag{5}$$

where $c_s(1\text{-}H_r)$ is the difference in the vapor concentration at the liquid–vapor interface of the droplet c_s, which is assumed to be its saturation value, and that far removed from the droplet surface $c_\infty = c_s H_r$, which is assumed to be its ambient value with H_r the relative humidity. An integral formulation was given by Stauber *et al.* and for ease of use, we provide an interpolation function for $f(\theta)$ (see the supplementary material, Eqs. S1–S3).

B. Non-isothermal model for sessile droplets of water

Recently, Nguyen *et al.*[22] reported an analytical solution of the sessile droplet evaporation coupled with interfacial cooling on a substrate heated at a constant temperature (non-isothermal model). Their results were uniquely quantified by a dimensionless evaporative cooling number, E_o, defined by

$$E_o = \frac{h_{ev} D c_s \varepsilon_c}{k_w}, \tag{6}$$

where $\varepsilon_c = 0.032\ \mathrm{K}^{-1}$, h_{ev} is the latent heat of evaporation, and k_w is the thermal conductivity of water. At 295 K, the evaporative cooling number of water is estimated to be $E_o = 0.11$; for methanol, $E_0 = 0.84$; and for acetone, $E_0 = 1.03$. This solution incorporating evaporative cooling is different to that of an isolated spherical droplet in free space. For the isolated case, where the droplet is not supported by a substrate, the heat flux into the droplet arises from the surrounding vapor rather than a substrate and involves a constant, $\varepsilon_T = h_{ev}Dc_s/k_a$, similar to Eq. (6) but using the thermal conductivity of air, k_a (see the work of Netz and Eaton[23] and Netz[24]).

Shen *et al.*[25] used the non-isothermal model of sessile droplet evaporation to provide a correction factor, $K(\theta, E_o)$, to the evaporation rate from the iso-thermal model (i.e., to the right-hand side of Eq. (5). This correction is expressed in an integral form and depends on the contact angle, θ, and the evaporative cooling number, E_o. We have evaluated this integral form and provide a simple interpolation for the range $0^\circ \le \theta \le 120^\circ$ for $E_o = 0.11$,

$$K(\theta, 0.11) = 1.000 - 0.000\,846\,621\theta + 0.000\,015\,849\,2\theta^2 - 9.086\,84 \times 10^{-8}\theta^3 - 5.842\,54 \times 10^{-9}\theta^4 + 8.674\,26 \times 10^{-11}\theta^5 - 3.837\,26 \times 10^{-13}\theta^6, \quad (7)$$

where θ is in degrees. [We note that eq. (4) in Shen *et al.*[25] has a typographical error and should use a sinh() and not a sin() in the numerator.] For contact angles above 120°, which is particularly useful for superhydrophobic surfaces, numerical evaluation of the integral equations is problematic and does not converge. A discussion of numerical simulations of Shen *et al.* and an interpolation of their results is given in the supplementary material (Sec. 2).

C. Water activity for sessile droplets of salt solutions

It has long been known that the presence of salt alters the concentration of water vapor at a water vapor surface to $c_s^{surface} = a_w(x)c_s$, where $a_w(x)$ is the water activity and $x = m_s/(m_s + m_w)$ is the mass fraction of the salt relative to the total mass of the droplet. The water activity is defined as the ratio of the vapor pressure of the solute/vapor pressure of pure water and is related to the Equilibrium Relative Humidity (ERH) of air surrounding a system by a_w = ERH/100, where the ERH is expressed as a %.

As discussed by Soulié *et al.*[6] and Seyfert *et al.*,[10] the evaporation rate of a sessile droplet of salt solution is reduced by a factor $(a_w - H_r)/(1 - H_r)$ compared to that of a pure sessile droplet of water. This introduces a time dependence because the activity of water depends on the salt concentration, which changes during evaporation and leads to an equilibrium droplet if $a_w = H_r$ is achieved, i.e., the ERH of the droplet becomes equal to the surrounding relative humidity. Seyfert *et al.*[10] noted that because there is a minimum value of water activity, $a_w^{\min} = a_w(x_{sat})$, determined by the saturated solution concentration, x_{sat}, some droplets containing salt may reach a stable volume. Thus, at 20 °C, the minimum water activity is $a_w^{\min} \approx 0.76$ and droplets, which start with $a_w > 0.76$, will not evaporate completely when $H_r > 75\%$. Seyfert *et al.*[10] identified three asymptotic regimes of sessile droplet evaporation. In regime I, for a relative humidity $H_r < 0.75$, the liquid phase evaporates completely and a dry deposit is created. In regime II, for relative humidity H_r in the upper vicinity of ~75%, the droplet volume remains stable at a maximum salt concentration. In regime III, for larger H_r, the droplet volume remains stable at larger volumes with a lower salt concentration due to a larger amount of liquid water.

D. Non-isothermal model for sessile droplets of salt solutions

The modification of the Picknett and Bexon[13] isothermal model for the evaporation of a sessile droplet of water [Eq. (5)] to include evaporative cooling and water activity due to the salt depressing the vapor pressure at the droplet–vapor interface is

$$\frac{dm}{dt} = -4\pi Dc_s(a_w - H_r)\left(\frac{3V}{\pi\beta(\theta)}\right)^{1/3} K(\theta, E_o)f(\theta), \quad (8)$$

where for the range $0^\circ \le \theta \le 120^\circ$ and $E_o = 0.11$, $K(\theta, 0.11)$ is given by Eq. (7) and $f(\theta)$ is given in the supplementary material in Sec. 1, Eqs. S1–S3. Equation (8) is similar to the equations previously provided by Soulié *et al.*[6] and Seyfert *et al.*,[10] but with the inclusion of the non-isothermal correction provided by Shen *et al.*[25] and with interpolating polynomials replacing integral formulations. The equation describes the rate of change of the mass of water, which is also the rate of change of the mass of the droplet.

Equation (8) can be re-written using the density, ρ_s, of the solution as

$$\frac{d(\rho_s V)^{2/3}}{dt} = -\frac{8\pi Dc_s}{3}\left(\frac{3}{16\pi}\right)^{1/3}\left(\frac{a_w - H_r}{\rho_s^{1/3}}\right)\left(\frac{K(\theta, E_o)}{\tilde{t}(\theta)}\right), \quad (9)$$

where

$$\tilde{t}(\theta) = \frac{\beta(\theta)^{1/3}}{2^{4/3}f(\theta)} \quad (10)$$

is a contact angle dependent factor in the iso-thermal model drop lifetime previously defined and discussed in Armstrong *et al.*[26] This factor has a maximum value of $\tilde{t}(\theta) = 1$ at $\theta = 90^\circ$ and decreases by not more than 11% of that value over the range $40^\circ \le \theta \le 180^\circ$. For this reason, the average evaporation rate and drop lifetime in the isothermal droplet of the water model tends to be insensitive to the precise value of the contact angle (provided it is sufficiently high) giving a quasi-constant contact angle mode of evaporation.

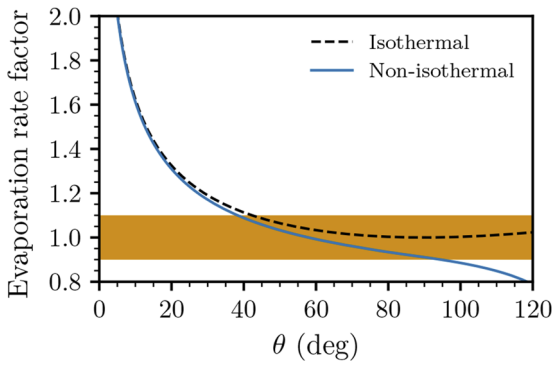

FIG. 1. Contact angle dependence of the evaporation rate factor, $\tilde{t}^{-1}(\theta)$, for pure water. The dashed line is the isothermal model, and the solid line is the non-isothermal model, which includes evaporative cooling. The orange shaded region represents a ±10% variation from 1.0 in the evaporation rate factor.

In contrast, as the contact angle decreases, the correction factor, $K(\theta, E_o)$, to the evaporation rate in Eq. (9) increases, and so their product increases. Figure 1 shows the evaporation rate factor,$\tilde{t}^{-1}(\theta)$, and the dependence on the contact angle, θ. The dashed line in Fig. 1 shows the iso-thermal model contact angle dependent evaporation rate factor with the limits for a ±10% variation shown as the shaded orange region. In contrast, the solid blue line showing the non-isothermal contact angle dependent evaporation rate factor, $\alpha(\theta, E_o) = K(\theta, E_o)/\tilde{t}(\theta)$, has a stronger variation in the higher contact angle range from 40° to 120°. Physically, this is as expected because the effect of evaporative cooling is strongest at higher contact angles, where the distance to transfer thermal energy from the substrate through the droplet to the droplet–vapor surface is larger on average.

On a SOCAL surface with an initial contact angle of $\theta = 104°$, the changes as the contact angle reduces to 60° and 40° are 2.8% and 10.8%, respectively, for the isothermal model. However, for the non-isothermal model, the changes are 10.5% and 18.8%, respectively. Thus, for a droplet of pure water, Eq. (9) predicts that the slope of a graph of $V(t)^{2/3}$ is approximately constant to within ±10% for contact angles above 40° but increases rapidly as the contact angle reduces below 40°. This corresponds to a quasi-constant contact angle mode of evaporation with a contact area that changes linearly with time. Thus, we expect the initial evaporation rate behavior to follow a quasi-constant contact angle regime with

$$\left(\frac{V(t)}{V_0}\right)^{2/3} \approx -\frac{8\pi D c_s}{3\rho_s^{2/3} V_0^{2/3}}\left(\frac{3}{16\pi}\right)^{\frac{1}{3}}\left\langle\left(\frac{a_w - H_r}{\rho_s^{1/3}}\right)\alpha(\theta, E_o)\right\rangle t + \left(\frac{\rho_o}{\rho_s}\right)^{2/3}, \tag{11}$$

where the angular brackets $\langle\cdots\rangle$ imply an average value over the relevant evaporation time and ρ_o and V_o are the initial density and volume of the droplet, respectively.

E. Time dependence of evaporation of droplets of salt solutions

For droplets of pure water, the water activity a_w and density ρ_s remain constant at their initial values, and so if the contact angle reduces as evaporation proceeds, the slope in a graph of $V(t)^{2/3}$ will become larger due to the contact angle factor, $\alpha(\theta, E_o)$. For sodium chloride (NaCl) salt solutions, the density term, $1/\rho_s{}^{1/3}$, decreases by at most ~6% and $1/\rho_s$ by at most ~17% as the concentration in a droplet increases. This decrease in the density factor partially compensates for increases in the slope of Eq. (11) caused by the contact angle dependent factor, $\alpha(\theta, E_o)$. For solutions of NaCl, the water activity a_w also decreases as the salt concentration increases[27,28] (Fig. 2) and can be described by a quadratic fit valid to within 3 decimal places for temperatures between 15 and 50 C.

$$a_w = 1 - 0.004\,721C - 0.000\,17C^2, \tag{12}$$

where C is the concentration (by % w/w). In regime I of Seyfert *et al*[10] ($H_r < 0.75$), the water evaporates completely from the droplet without ever reaching a value of a_w giving an equilibrium with the surrounding relative humidity and so leaves a salt deposit. In this case, as a droplet approaches the end of its lifetime, we would expect the slope in Eq. (11) to become steeper due to the contact angle dependent factor $\alpha(\theta, E_o)$. In regimes II and III, the droplet eventually reaches an equilibrium volume due to the term $(a_w - H_r)$ and so the slope in Eq. (11) should become shallower.

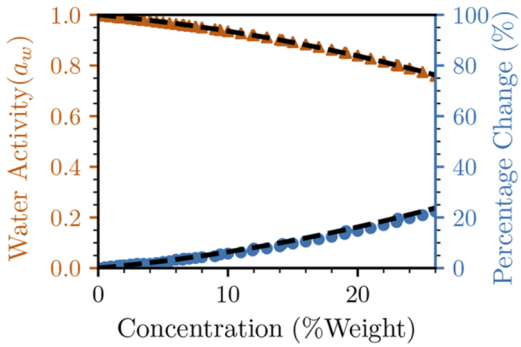

FIG. 2. Water activity, a_w, dependence on the concentration of the NaCl solution. The orange triangles show the plotted data for water activity as a function of the concentration (left axis),[27–29] and the dotted line shows the quadratic fit [Eq. (12)]. The blue circles show the percentage drop of water activity as a function of the concentration calculated from the previous references. The dotted line shows a quadratic fit.

III. EXPERIMENTAL METHODS

A. Surface preparation

The different surface coatings used in our experiments were SOCAL, PEGylated, Glaco, polytetrafluoroethylene (PTFE), and SU8. We also used a bare glass substrate as a high hysteresis low contact angle substrate. They were all chosen to give a wide range of different static contact angles and contact angle hysteresis values (Table I).

To achieve a constant contact angle evaporation, which requires surfaces that exhibit no contact line pinning, we used SOCAL surfaces. The surfaces are based on the work of McCarthy *et al.* using modifications by Armstrong *et al.* and are smooth, hydrophobic (CA > 90°), and have low CAH (~2°).[11,12] These surfaces were produced by plasma treating a chemically cleaned glass slide to activate the surface. The slide was placed in a plasma cleaner (Henniker) at 30% power for 20 min using air as the reactive gas. The slide was then dip coated in a reactive solution made of a 100:10:1

TABLE I. Table of value for surface experiments.

Surface coating	Contact angle (°)	CAH (°)	No. of droplets studied	Droplets producing crystals at $t < 8000$ s)
SOCAL	105	<2	25	0
PEG	35–45	0.5–3.5	25	7
Glaco	170	5	5	0
PTFE	120	12	3	0
SU8	75	25	4	1
Glass	9.5	High	3	3

mass ratio of isopropyl alcohol, dimethyoxydimethylsilane, and sulfuric acid, respectively. The slide was dipped in the solution and held for 10 s. It was then withdrawn at 3 mm s^{-1} before being left to react in a chamber at a relative humidity of 60 ± 1% for 20 min. The excess unreacted material was washed away with deionized water, isopropyl alcohol, and toluene and then air dried. The surfaces were characterized by an averaged value of three hysteresis measurements and were deemed to be fit for use in the evaporation experiments when they achieved the values of <2° CAH and standard deviation of < ± 0.5°.

To achieve a CCA mode of evaporation on a smooth and hydrophilic surface (CA < 90°), we used a PEGylated coating with low CAH (~3°);[16,30] we refer to these PEGylated surfaces as our PEG surfaces throughout. The PEG surfaces were produced by activating the surface of a cleaned glass slide in a plasma oven for 40 min at 60 W power. The activated surfaces were then reacted in a reagent solution of toluene, 2-[methoxy(polyethyleneoxy)6-9propyl]trimethoxysilane, and hydrochloric acid by immersing the sample in a bath of the reagent for 18 h. The samples were then rinsed with deionized water, isopropyl alcohol, and toluene to remove any unreacted material.

The superhydrophobic Glaco sample was made by spraying a cleaned glass slide with a Glaco Mirror Coat™ and leaving it to dry in air for an hour. The spraying process was repeated 5 times to build a more uniform structure across the sample. The Glaco coated surfaces are referred to as Glaco surfaces throughout.

The polytetrafluoroethylene (PTFE) sample was prepared by spinning a PTFE solution (Teflon™ AF1600) onto a cleaned glass slide at 500 rpm for 10 s and then 2000 rpm for 1 min and by baking at 155 °C for 20 min. The samples coated with SU8 photoresist were made by spin coating SU8-3035 on a 3″ silicon wafer at 500 rpm for 10 s and then 2000 rpm for 30 s. They were then baked at 95 °C for 10 min flood exposed at 5000 mJ/cm^2 and post-baked for 2 min at 95 °C

For experiments that used a bare glass substrate, the glass slide (Sigma-Aldrich) used was taken fresh from the packet. The hysteresis of the glass slide was high, and it could not be characterized through the same stringent method as the other samples due to the high wettability and low contact angle of the surface.

B. Salt solution preparation

NaCl solutions used 99.9% pure reactant grade sodium chloride salt (Sigma-Aldrich) and ultra-pure water (Sigma-Aldrich). 10 ml solutions were prepared in a 12 ml scintillation vial, and the solution was mixed using a vortexer (Fisher Mini Vortexer) for 2 min continuously to ensure homogeneous dissolution of the salt.

C. Contact angle hysteresis measurements

The pinning-free properties of these surfaces were characterized through CAH measurements. These measurements were made at high relative humidities in line with the contact-line relaxation method demonstrated by Barrio-Zhang *et al.*[31]

D. Droplet imaging, deposition, and humidity control

To control the evaporation conditions around the droplet, a bespoke droplet shape analysis experiment was constructed. The experiment uses a 12 MP camera (Raspberry PI) with a microscope lens (Raspberry Pi C-mount microscope lens) to capture an image of the droplet. The recording quality was 1080p to reduce analytical errors, and single images were captured at 10 s intervals (0.1 FPS). The open source software used (PyDSA) tracks the contact radius, r, throughout the evaporation and calculates the contact angle, θ, from a fit to a third-degree polynomial between the spherical cap fitting and the set baseline. From these data, the volume of the droplet can be calculated assuming the axial symmetry. A microfluidic syringe pump (Cellix Exigo) is used to accurately dose the droplets of 4 ± 0.4 μl. A PID temperature-controlled stage (Thorlabs, PTC1/M) was used to control the temperature, and a bespoke humidity controller was used to control the humid environment. The temperature of the surface was regulated to ±0.2 °C, and the glass surface of the samples was assumed to be in thermal equilibrium with the heated surface. The humidity controller was regulated to ±1% relative humidity. We used four air inlets and the hole for the needle as the outlet. This prevents any humidity gradients from forming within the chamber.

E. Single droplet water evaporation on SOCAL

To determine that CCA evaporation was achievable on SOCAL surfaces, we used water as a baseline for the evaporation dynamics. An amount of 4 μl droplets of ultra-pure water (Sigma-Aldrich) was evaporated on SOCAL surfaces at 25 °C and 60% relative humidity (red squares). The captured images of the droplets were analyzed using a bespoke open-source tool (pyDSA) to calculate the instantaneous contact angle and contact radius. Using the contact radius data and contact angle, assuming a spherical cap of the droplet, we can calculate the volume of the droplet numerically. From these data, the evaporation dynamics were analyzed and the evaporation mode was determined by plotting $(V/V_0)^{2/3}$ as a function of time. According to Eq. (11), this plot should show a linear relationship for CCA evaporation. By first ensuring that a CCA evaporation is achievable using water as the fluid, we can observe the effects of the non-pure liquid droplet as the surface behavior is already known.

F. Single saline droplet variable humidity evaporations

To evaluate the response of saline solutions to different humidities, droplets of 0.108 weight fraction saline solution were taken at different relative humidities. A 4 μl droplet of 0.108 weight fraction solution was evaporated at 40%, 55%, 60%, 65%, and 75% relative humidity and at a fixed temperature of 25 °C. Each different droplet was evaporated at a different location on a SOCAL sample. The evaporation dynamics were observed in real-time and performed until the volume of the droplet remained stationary.

G. Single saline droplet variable concentration evaporations

To investigate the effects of water activity on evaporation, droplets of varied concentrations from 0.008 to 0.108 weight fraction were evaporated at 60% relative humidity and 25 °C. Each condition was repeated three times and evaporated for at least 8000 s. The experiments were all run on the same SOCAL sample and performed non-sequentially to prevent any aging effects of the surface.

H. Single saline droplet variable surface evaporations

To study the effect of the contact angle and contact angle hysteresis on whether the droplet is crystallized or not, we used a variety of surfaces with different contact angle and contact angle hysteresis properties (Table I) and evaporated droplets under the same conditions as for droplets on SOCAL coated glass.

I. Multiple droplet (multiplexed) crystallization study

PEG and SOCAL surfaces have very low contact angle hysteresis but very different wettability. To test the effect of the surface on the stability of the droplets, we carried out a study involving the evaporation of arrays of multiple droplets. The conditions were kept the same as in the previous study; however, the dosing and observation of the evaporations changed, for the SOCAL, arrays of 10 or 5 droplets of 4 μl were deposited in a zig-zag pattern to relatively reduce their interference of the local humidity around the droplet (approximately one droplet diameter apart).The distance between the droplets at this distance coupled with the long duration of the experimental observations ensures that at the end of the observations, all saline droplets are in equilibrium with the surrounding vapor phase. These arrays were then left for 9000 s, an extra 1000 s to the singular droplet for extra confidence in the assertions. After the 9000 s, the number of crystals in the array was counted. For the PEG surfaces, five droplets were deposited and observed under the same conditions and once 25 droplets had been observed for each surface, we compared the number of crystals deposited. The surfaces were chosen for their comparative hysteresis values (see Table I).

IV. RESULTS AND DISCUSSION

A. Response of saline droplets to humidity

To investigate the ability of smooth low contact line pinning surfaces such as SOCAL to mitigate the heterogeneous nucleation of crystals, we first performed the experiments to determine how the relative humidity of the chamber affects the evaporation of the droplets and crystal formation. We placed 0.108 weight fraction droplets of initial volume $V_o = 4\mu l$ on a smooth SOCAL surface (CA 105 ± 1°, CAH 1.11 ± 0.28) and adjusted the relative humidity to 55%, 60%, 65%, and 75% (preliminary results on 40% and 50%; all crystallized). Figure 3(a) shows $V/V_o{}^{2/3}$ as a function of time for each different humidity. For a droplet on a SOCAL surface, which has been shown to be smooth and stable,[11] it is possible to create droplets (b) with a stable volume for at least 8000 s. As shown in Fig. 3(a), the droplet reaches an equilibrium volume with the evaporation rate eventually reaching zero. This is consistent with Eq. (11) and the $(a_w - H_r)$ term reaching zero as the water activity becomes equal to the surrounding relative humidity. The lower humidity stable droplets including 55%, 60%, and 65% suggest that the water activity at the surface of the droplet can be much lower than the limiting value of $H_r = 0.76$ previously mentioned for a sessile droplet.[10]

It can also be seen that as expected, the volume at which the droplet stabilizes is dependent on the relative humidity. This shows that SOCAL surfaces are able to mitigate heterogeneous nucleation and stabilize the droplets of the constant volume at a humidity as low as 55% which is much lower than the expected deliquescence limit of ~75%.[8]

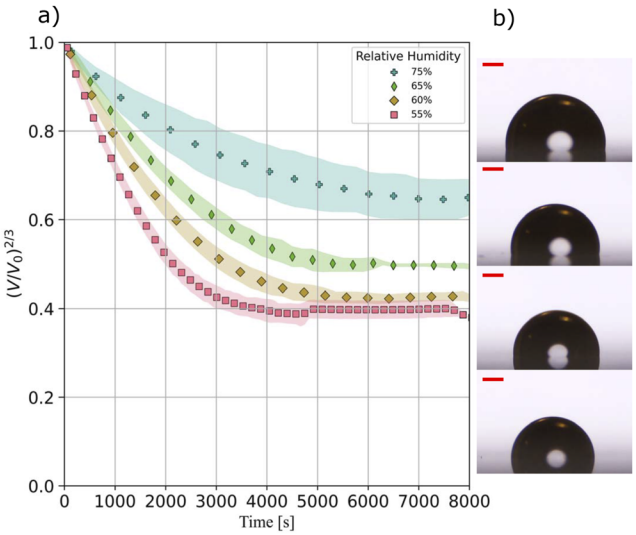

FIG. 3. (a) Effect of the relative humidity on the volume variation vs time of 0.108 weight fraction NaCl droplets at 25 °C. (b) Final saturated droplets corresponding to each relative humidity ordered vertically by the legend shown in the figure with the scale bars showing 0.4 mm (a). Shaded area represents the standard deviation of three different independent experiments.

B. Effect of the initial concentration on the stable volume

The final volume of an evaporating droplet is also determined by the weight fraction of salt in the solution at which the water activity has equalized with the relative humidity. This final volume will,

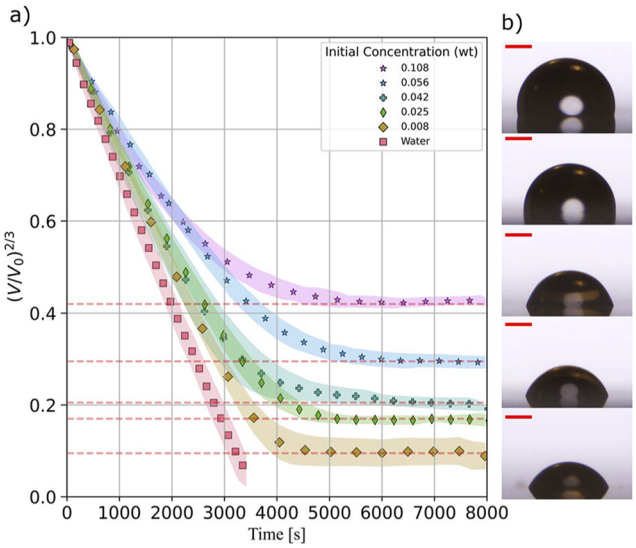

FIG. 4. (a) Observed changes in $(V/V_0)^{2/3}$ vs time for various concentrations of saline solutions shown in the legend at 60% RH. (b) Liquid droplets of the final stable volumes ordered vertically from the largest initial concentration to least excluding a water droplet which does not stabilize. Scale bars show 0.4 mm.

thus, be dependent on the initial weight fraction of salt in the droplet. Therefore, varying the initial weight fraction of salt in the solution leads to different final volumes. Figure 4 shows $(V/V_0)^{2/3}$ as a function of time for droplets with different initial weight fractions. The red squares show the calibration experiment for water on SOCAL, showing a CCA diffusion limited evaporation. Figure 7(a) shows that it is possible to stabilize droplets with an initial weight fraction as low as (0.008) (brown diamonds) and that increasing the weight fraction increases the final, stable volume. Figure 7(b) shows that the stable droplets are indeed liquid solutions even when the final volume is only 3% of the original volume. We note that perturbing the stable droplets with the needle did not induce crystallization and that the droplets did remain liquid [see the supplementary material, Fig. S4 (Multimedia View)]. In addition, it is shown that for low weight fraction, the droplets follow the diffusion limited model of evaporation [Eq. (11)][13] and only deviate as the volume gets close to the stable volume. However, for much higher initial weight fraction, the droplet deviates from diffusion limited evaporation almost immediately and follows a different dynamic path to the stable volume.

C. Evaporation on different surfaces

We assume that for sessile droplets in contact with a surface, crystal nucleation takes place due to micro or nanoscopic surface roughness. SOCAL surfaces have been shown to be very smooth and to have very low contact angle hysteresis hindering crystal nucleation for relative humidity concentrations below that established by its water activation coefficient as shown in earlier Sec. IV A. To test the ability of other coated surfaces to mitigate heterogeneous nucleation, we recorded evaporation sequences for 4 μl droplets of a 0.108 weight fraction salt solution, at 60% relative humidity, on several different substrates, namely, PEG, PTFE, Glaco, and SU8 with static contact angles and contact angle hysteresis reported in (Table I). Figure 5 shows the outcome of evaporation sequences on these surfaces. $(V/V_0)^{2/3}$ as a function of time is shown in the central graph panel, and the left and right image strips show the initial droplet and the final droplet shapes, respectively. From the evolution of the volume in time data reported in Fig. 5, there is a rather good agreement and all of the data collapse for substrates with contact angles equal to or below 120°. In addition, we can see from the volumetric data that we were able to stabilize saline droplets, without crystallization and for at least 8000 s, on all of the surfaces. For PEG, SOCAL, SU8, and PTFE coated surfaces, the static average contact angle during the evaporation is between 38° and 110° [see Fig. 5(b) inset]. For the Glaco superhydrophobic surface, the average contact angle is ≈150°. According to Fig. 1 for the non-isothermal model of evaporation, we would expect to see a change in the evaporation rate of ~20% between 38° and 110° (Fig. 1). This is not very evident for PEG, SOCAL, PTFE, and SU8, during the volume loss phase of the evaporation in Fig. 5. This could be because for the 20% change in the evaporation rate expected on these surfaces, the water activity is the dominant effect controlling the evaporation rate. There is, however, a significant change in the evaporation rate for the droplet on the Glaco coated surface. Although 150° is outside the range of the plot in Fig. 1, we can see that the evaporation rate begins to significantly deviate from the isothermal model and slows the evaporation as the contact angle gets very large. This would account for the significant change in the evaporation rate seen for the droplet on a Glaco coated surface.

The ability to stabilize a droplet on different surfaces is more difficult to achieve as the hysteresis values increase. To test our hypothesis that low CAH surfaces with constant contact angle evaporation may suppress the occurrence of crystallization, we performed studies using the droplet arrays on the SOCAL and PEG surfaces (see experimental methods). Table I shows the outcome of these experiments, along with data for the experiments on other surfaces with >2° CAH.

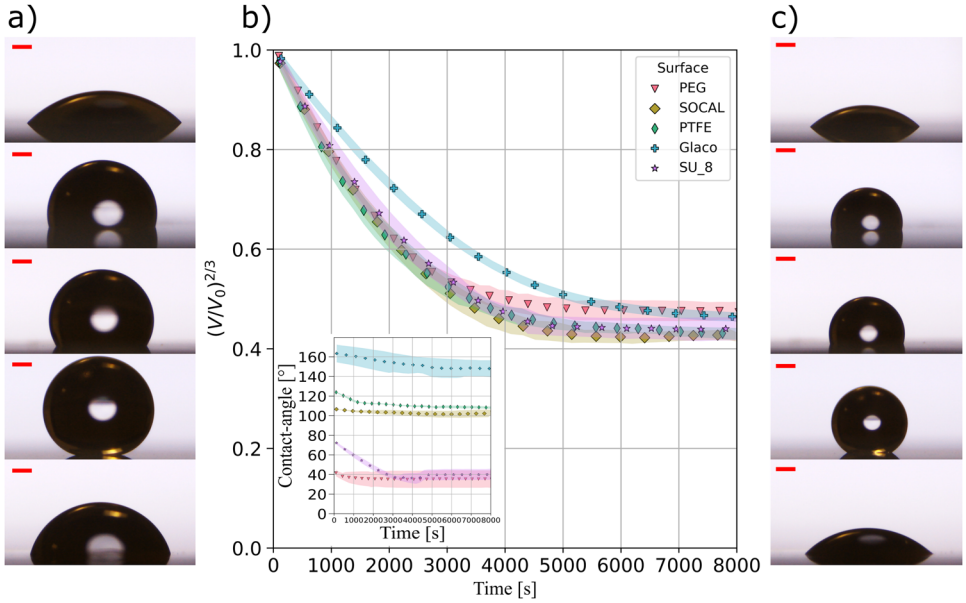

FIG. 5. Surface effects on saline droplets. (a) Initial shapes of the droplets on the surfaces. From top to bottom, PEG, SOCAL, PTFE, Glaco, and SU8. (b) Main graph, normalized droplet volumes as function of time, and inset droplet contact angles as a function of time. The key is the same in both graphs. (c) Final droplet shapes; top to bottom images are same as in panel a), with scale bars showing 0.2 mm.

For SOCAL surfaces, 25 of the 25 droplets in the array remained stable and showed no crystallization for at least 9000 s, and in one experiment, we were able to stabilize a single droplet for at least 20 320 s (see supplementary Figs. S2 and S3). For PEG surfaces, the number of stable droplets dropped to 18 of the 25. The difference in the fraction of the droplets that formed crystals might be attributed to a much larger contact footprint giving a higher probability of nucleation sites and/or to the different spatial distribution of the evaporative flux generating local concentrations gradients near the contact line.[32] Although Glaco and PTFE surfaces showed no crystals and stable droplets for every experiment (only 3 of each) at $t < 8000$ s, they both proved that it is very difficult to produce stable droplets in the long term. We were not able to stabilize a droplet on any of the glass surface experiments.

D. Weight fraction and water activity analytical model

The nature of the evaporation paths of droplets toward the final stable volume can be explained by the increasing concentration as the water evaporates, which, in turn, decreases its activity. The percentage weight fraction of a droplet of known molarity is given by

$$wt(V) = \frac{MM_{salt} V_i}{V(t)_{drop} \rho_{sol}}, \tag{13}$$

where M is the molarity of the solution used in the experiment, M_{salt} is the molar mass of the salt, V_i is the initial volume of the droplet, $V(t)_{drop}$ is the dynamic volume of the droplet, and ρ_{sol} is the density of the droplet solution. To analyze how the concentration and water activity vary as a function of the droplet volume, we use an upper and lower bound for the density in Eq. (13).

Figure 6(a) shows an analytical plot of the weight fraction as a function of $(V/V_o)^{2/3}$ for droplets with different initial weight fractions matching those in the experiments. The bands represent the space bounded by how weight fraction changes given a minimum and maximum density. In the case of saline droplets, the minimum possible density would be that of pure water (1000 kg/m^3) with no salt in the solution (black dotted line on each band). Assuming that creating a very smooth surface mitigates heterogeneous crystallization, we assume supersaturation of the droplets, as previously mentioned. Since the earlier experiments were performed at a relative humidity of 60%, corresponding to $H_r = 0.6$, the weight fraction of NaCl at which the water activity matches the relative humidity is 0.4. Thus, the upper limit of the density used in this plot is 1295 kg/m^3, equivalent to a saline solution of 0.40 weight fraction (this value is extrapolated from density vs weight fraction data which is plotted between 0 and 0.26 weight fraction; see the supplementary material, Fig. S1).[29] The bands in Figs. 5 and 6 show the regions bounded by using these two densities in Eq. (13).

By substituting the weight fraction as a function of density [Eq. (13)] into the quadratic fit to water activity [Eq. (12)], we can see how the water activity changes as a function of volume [Fig. 6(b)]. The red dotted line in Fig. 6(b) is the water activity at the expected deliquescence limit at $a_w = 0.75$, and the green line is the water activity at $a_w = 0.60$. Using the analytical solution, it is possible to predict the final volume for a stable volume droplet on the SOCAL surface and compare it with the experimental measurements. The crossing points of the different initial concentration bands with the horizontal dotted green line should coincide with a steady state volume of the final droplet.

Figure 7 shows the data for all the experiments for different surfaces as well as the experiments for different concentrations of the saline solution. The yellow filled region shows the upper and lower bounds which are determined using the same densities as reported in Fig. 6, this shows that the theoretical prediction is in good agreement with the experimental data. Figure 7(a) shows the final volume of the droplet when it is stable as a function of the initial weight fraction. The blue filled circles show the concentration experiments carried out only on SOCAL surfaces, and the orange triangles show the experiments for different surfaces for which the highest of the

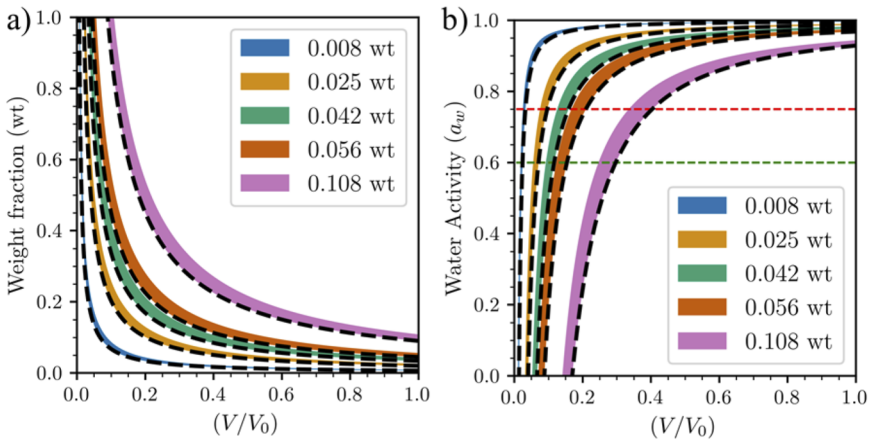

FIG. 6. (a) Expected weight fraction as a function of (V/V_0) for a 4 μl droplet of NaCl solution. (b) Water activity for various initial percentage weight solutions as a function of volume. Each colored density band corresponds to a lower bound (black dotted line) corresponding to the initial density of the solution (1000 kg/m^3) and an upper bound corresponding to the maximum density of the solution at 0.4 weight fraction (1295 kg/m^3). The horizontal red dotted line indicates when the water activity is equivalent to the expected value for a sodium chloride solution at 0.75, and the green dotted line indicates when the water activity matches $H_r = 0.60$ in the experiments.

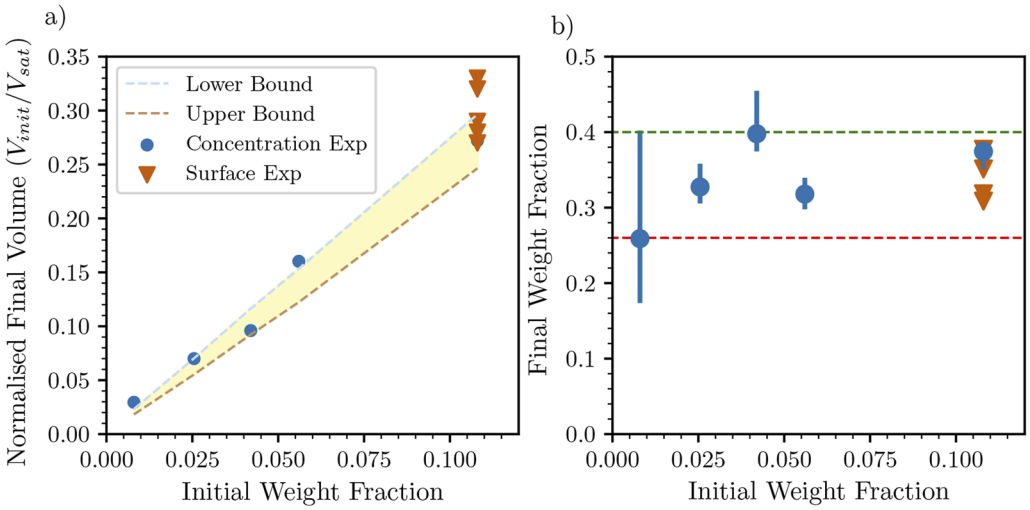

FIG. 7. (a) Final normalized saturation volume of the droplet (V_{init}/V_{sat}) as a function of the initial weight fraction. The blue circles indicate the experimental data, and the blue and orange dotted lines represent the upper and lower bounds, respectively. The downward orange triangles indicate data for non-SOCAL surfaces. (b) Final weight fraction as a function of the initial weight fraction. All experimental and theoretical data shown are for 60% relative humidity. The green dotted line represents the supersaturation equilibrium concentration, and the red dotted line represents the expected 26% saturation concentration.

saline concentrations was chosen. The data in the experiments are in good agreement with the analytical model; hence, we can predict the final volume of the droplets. From the surface data, it is also clear that this model works for different initial contact angles. Figure 7(b) shows the values of the concentrations of the final droplets as a function of the initial weight fraction. This concentration is calculated using Eq. (13) with the density set to 1147.5 kg/m^3, which is the average density used in the model. The horizontal red dotted line in Fig. 7(b) shows the expected saturation concentration of 26% for an NaCl solution. All the data in Fig. 7(b) show that the droplets that remain on the surface are supersaturated when stable. According to the model, we would expect the droplet to stabilize at a concentration of 0.40 (green dotted line) weight fraction salt (equivalent to 0.60 weight fraction water) if the water activity has reached equilibrium with the surrounding environment. In all experiments, the final concentration of the stable droplet is above the expected concentration of 26%. We note that the smallest initial concentration has a large error bar because, as shown in Fig. 6(a), a very small error in volume calculation, arising from axisymmetric assumptions, can lead to large errors in the weight fraction. This effect becomes smaller as the initial concentration increases.

V. CONCLUSION

In this work, we have shown that it is possible to create sessile droplets of a supersaturated sodium chloride salt solution whose volume remains constant on different solid surfaces and at different relative humidities without crystallization over significant periods of time. This relative humidity, at which the droplet stabilizes, is above the expected equilibrium relative humidity for a NaCl solution and appears to occur when the water activity has equalized with the surrounding humidity. We have also shown that on a smooth surface of SOCAL, with a relatively high static contact angle (105°) and a low contact angle hysteresis (<2°), it is possible to create stable droplets at a relative humidity as low as 55%. At a slightly higher relative humidity (60%), this is a highly reproducible effect. On PEG surfaces, we have achieved similar results to that of SOCAL at relative a relative humidity of 60% but with slightly lower reproducibility of stable droplets on larger timescales. We have shown that, although more difficult, other surface coatings are capable of creating stable droplets at 60% relative humidity. On superhydrophobic surfaces, we show a significant deviation from the diffusion limited evaporation model throughout the droplet lifetime and we attribute this to a lower water activity and non-isothermal evaporation. The deviation from diffusion limited evaporation to a stable droplet is due to the decreasing water activity within the droplet and due to an increase in the concentration of salt as the droplet evaporates. We have also presented an analytical model that predicts the final stable volume of the droplets and have shown that it is in good agreement with the experiments.

SUPPLEMENTARY MATERIAL

In the supplementary material, we provide the details of a new interpolation for the function $f(\theta)$ from the data of Stauber *et al.*, to take account in a common notational format of the dependence of the concentration gradient of the vapor, between the surface of the droplet and its surroundings, on the contact angle arising from different models. We also provide an interpolation for the non-isothermal evaporation factor for angles greater than 120°. The data plot of the saline solution density as a function of concentration and the extrapolation used in the analytical model in Eq. (13) is included, and we also include an extra plot of the very long evaporation experiment mentioned in Sec. IV C as well as the droplet images from the same experiment.

ACKNOWLEDGMENTS

GM is grateful to Dr. Yongpan Cheng for data and discussions on the evaluation of the correction factor for the evaporation rate of a non-isothermal droplet. AJ would also like to thank Dr. Hernán Barrio-Zhang and Michele Pelizzari for providing PEGylated and Glaco surfaces, surface preparation training, and valuable insight. SA would like to acknowledge the support of the Engineering and Physical Sciences Research Council (Grant Number EP/T025158/1).

AUTHOR DECLARATIONS

Conflict of Interest

The authors have no conflicts to disclose.

Author Contributions

Alex Jenkins: Conceptualization (supporting); Data curation (lead); Formal analysis (lead); Investigation (equal); Methodology (equal); Software (equal); Writing – original draft (equal); Writing – review & editing (equal). **Gary G. Wells**: Conceptualization (equal); Methodology (lead); Project administration (lead); Supervision (lead); Writing – original draft (lead); Writing – review & editing (lead). **Rodrigo Ledesma-Aguilar**: Conceptualization (equal); Methodology (equal); Supervision (equal); Writing – review & editing (equal). **Daniel Orejon**: Supervision (equal); Writing – review & editing (equal). **Steven Armstrong**: Conceptualization (supporting); Data curation (supporting); Formal analysis (supporting); Methodology (supporting); Writing – review & editing (equal). **Glen McHale**: Conceptualization (equal); Investigation (equal); Project administration (equal); Supervision (equal); Writing – original draft (equal); Writing – review & editing (equal).

DATA AVAILABILITY

The data that support the findings of this study are available from the corresponding author upon reasonable request.

REFERENCES

[1] H. Yoo and C. Kim, Colloids Surf., A **468**, 234 (2015).
[2] R. Bhardwaj and A. Agrawal, Phys. Fluids **32**, 111706 (2020).
[3] S. Mashaghi, A. Abbaspourrad, D. A. Weitz, and A. M. van Oijen, TrAC - Trends Anal. Chem. **82**, 118 (2016).
[4] M. C. Yuen and L. W. Chen, Int. J. Heat Mass Transfer **21**, 537 (1978).
[5] Z. Wang, D. Orejon, Y. Takata, and K. Sefiane, Phys. Rep. **960**, 1 (2022).
[6] V. Soulié, S. Karpitschka, F. Lequien, P. Prené, T. Zemb, H. Moehwald, and H. Riegler, Phys. Chem. Chem. Phys. **17**, 22296 (2015).
[7] M. S. Rahman and T. P. Labuza, *Handbook of Food Preservation* (CRC Press, 2007), p. 1.
[8] C. Peng, L. Chen, and M. Tang, Fundam. Res. **2**, 578 (2021).
[9] S. T. Martin, Chem. Rev. **100**, 3403 (2000).
[10] C. Seyfert, J. Rodríguez-Rodríguez, D. Lohse, and A. Marin, Phys. Rev. Fluids **7**, 023603 (2021).
[11] L. Wang and T. J. McCarthy, Angew. Chem., Int. Ed. **55**, 244 (2016).
[12] S. Armstrong, G. McHale, R. Ledesma-Aguilar, and G. Wells, Langmuir **35**, 2989 (2019).
[13] R. G. Picknett and R. Bexon, J. Colloid Interface Sci. **61**, 336 (1977).
[14] F. K. A. Gregson, J. F. Robinson, R. E. H. Miles, C. P. Royall, and J. P. Reid, J. Phys. Chem. B **123**, 266 (2019).
[15] A. P. Olsen, R. C. Flagan, and J. A. Kornfield, Rev. Sci. Instrum. **77**, 073901 (2006).
[16] H. Cha, H. Vahabi, A. Wu, S. Chavan, M. K. Kim, S. Sett, S. A. Bosch, W. Wang, A. K. Kota, and N. Miljkovic, Sci. Adv. **6**, eaax0746 (2020).
[17] H. Zhao, C. A. Deshpande, L. Li, X. Yan, M. J. Hoque, G. Kuntumalla, M. C. Rajagopal, H. C. Chang, Y. Meng, S. Sundar, P. Ferreira, C. Shao, S. Salapaka, S. Sinha, and N. Miljkovic, ACS Appl. Mater. Interfaces **12**, 12054 (2020).
[18] A. K. Halvey, B. Macdonald, K. Golovin, M. Boban, A. Dhyani, D. H. Lee, J. W. Gose, S. L. Ceccio, and A. Tuteja, ACS Appl. Mater. Interfaces **13**, 53171 (2021).
[19] Y. Chen, X. Yu, L. Chen, S. Liu, X. Xu, S. Zhao, S. Huang, and X. Tian, Environ. Sci. Technol. **55**, 8839 (2021).
[20] J. M. Stauber, S. K. Wilson, B. R. Duffy, and K. Sefiane, Langmuir **31**, 3653 (2015).
[21] H. Y. Erbil, G. McHale, and M. I. Newton, Langmuir **18**, 2636 (2002).
[22] T. A. H. Nguyen, S. R. Biggs, and A. V. Nguyen, Langmuir **34**, 6955 (2018).
[23] R. R. Netz and W. A. Eaton, Proc. Natl. Acad. Sci. U. S. A. **117**, 25209 (2020).
[24] R. R. Netz, J. Phys. Chem. B **124**, 7093 (2020).
[25] Y. Shen, F. Kang, Y. Cheng, K. Zhang, and Y. Sui, Int. J. Therm. Sci. **172**, 107284 (2022).
[26] S. Armstrong, G. McHale, R. Ledesma-Aguilar, and G. G. Wells, Langmuir **36**, 11332 (2020).
[27] J. Chirife and S. L. Resnik, J. Food Sci. **49**, 1486 (1984).
[28] V. Gekas, C. Gonzalez, A. Sereno, A. Chiralt, and P. Fito, Int. J. Food Prop. **1**, 95 (1998).
[29] A. I. Simion, C. Grigoraş, and A. Roşu, J. Agroaliment. Process. Technol. **21**, 41 (2015).
[30] A. Papra, N. Gadegaard, and N. B. Larsen, Langmuir **17**, 1457 (2001).
[31] H. Barrio-Zhang, É. Ruiz-Gutiérrez, S. Armstrong, G. McHale, G. G. Wells, and R. Ledesma-Aguilar, Langmuir **36**, 15094 (2020).
[32] R. D. Deegan, O. Bakajin, and T. F. Dupont, Nature **389**, 827 (1997).